Chinese Chemical Letters 35 (2024) 109085

Contents lists available at ScienceDirect

Chinese Chemical Letters

journal homepage: www.elsevier.com/locate/cclet

Chiral induction and Sb^{3+} doping in indium halides to trigger second harmonic generation and circularly polarized luminescence

Yongjing Deng[a], Feiyang Li[b], Zijian Zhou[a], Mengzhu Wang[a], Yongkang Zhu[a], Jianwei Zhao[c], Shujuan Liu[a,*], Qiang Zhao[a,*]

[a] State Key Laboratory of Organic Electronics and Information Displays & Jiangsu Key Laboratory for Biosensors, Institute of Advanced Materials (IAM) & Institute of Flexible Electronics (Future Technology), Nanjing University of Posts & Telecommunications (NJUPT), Nanjing 210023, China
[b] School of Environmental and Chemical Engineering, Jiangsu University of Science and Technology, Zhenjiang 212100, China
[c] Shenzhen HUASUAN Technology Co., Ltd., Shenzhen 518000, China

ARTICLE INFO

Article history:
Received 24 July 2023
Revised 25 August 2023
Accepted 11 September 2023
Available online 12 September 2023

Keywords:
Hybrid metal halides
Self-trapped excitons
Chiral induction
Second-harmonic generation
Circularly polarized luminescence

ABSTRACT

Recently, organic-inorganic hybrid metal halides (HMHs) have attracted extensive attention as promising multifunctional materials by virtue of their structural diversity and tunable photophysical properties. However, it remains a challenge to design HMHs with specific functions on demand. Herein, by introducing *R*/*S*-methylbenzylamine (*R*/*S*-MBA) and doping Sb^{3+}, we have achieved both second harmonic generation (SHG) and circularly polarized luminescence (CPL) properties in lead-free indium halides. The introduction of chiral organic cations can break the symmetry and induce the indium halides to crystallize in the chiral space group. The Sb^{3+} with ns^2 electronic configuration can serve as the dopants to promote the formation of self-trapped excitons, so as to activate highly efficient luminescence. As a result, the as-prepared Sb^{3+} doped $(R/S\text{-MBA})_3InCl_6$ show not only SHG responses but also CPL signals with luminescence dissymmetry factor of -5.3×10^{-3} and 4.7×10^{-3}. This work provides a new inspiration for the exploitation of chiral multifunctional materials.

Molecular crystalline materials that couple multiple properties have exhibited broad application prospects in the field of integrated optoelectronic devices due to their long-range ordering, regular shapes, and low defect density [1,2]. Among them, organic-inorganic hybrid metal halides (HMHs) have attracted much attention by virtue of their unique hybrid compositions, flexible crystal structures and designable photophysical properties [3–7]. As we know, the photophysical properties of HMHs are greatly related to their crystal structures [8]. Symmetry is one of the basic properties of crystals, and plays a crucial role in constructing structure-property relationships. Some studies have shown that the symmetry breaking in crystalline materials can introduce some novel function like nonlinear optical effect, spin selectivity effect and bulk photovoltaic effect [9,10]. Given that regular HMHs usually crystallize in centrosymmetric space groups, the development of non-centrosymmetric HMHs is of great interest for multifunctional applications [11].

Chiral induction, introducing chiral molecules as the templating cations, has been demonstrated as a feasible strategy to reduce the structure symmetry [12,13]. In 2003, Billing *et al.* reported the first case of chiral HMHs, (*S*-MBA)$PbBr_3$ (MBA = methylbenzylamine), in which chiral amines were introduced into the inorganic $[PbBr_3]^-$ framework as templating cations [14]. However, the chiral optical properties have not been explored. Until 2017, the circular dichroism (CD) signals of chiral HMHs were first discovered by Moon *et al.* in two-dimensional $(R/S\text{-MBA})_2PbI_4$ [15]. Since then, numerous metal halides have been developed by changing the hybrid compositions, and exhibit broad application prospects [16,17]. For example, Li *et al.* reported chiral $(R/S\text{-MBA})_2PbI_4$ crystals, which exhibited sensitive circularly polarized light detection and circularly polarized luminescence (CPL) [18]. Subsequently, Duan *et al.* reported the first example of two-photon absorption-based upconverted CPL [19]. Benefiting from the inherent non-centrosymmetric structure, chiral HMHs also possess second harmonic generation (SHG) activity. For example, Luo *et al.* reported a chiral HMH, (*R*-3-aminopiperidine)$PbCl_4 \cdot H_2O$, which exhibited distinct CD and SHG responses [20]. Recently, Zhang *et al.* reported the chirality-dependent SHG effect in (*R*/*S*-3-aminopiperidine)PbI_4 [21]. However, the current investigation on chiral HMHs mainly focuses on

* Corresponding authors.
E-mail addresses: iamsjliu@njupt.edu.cn (S. Liu), iamqzhao@njupt.edu.cn (Q. Zhao).

https://doi.org/10.1016/j.cclet.2023.109085
1001-8417/

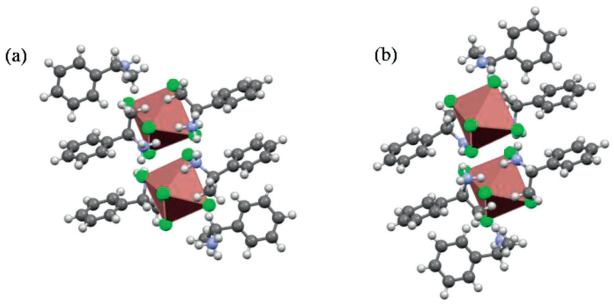

Fig. 1. Crystal structures of (a) (*R*-MBA)$_3$InCl$_6$ and (b) (*S*-MBA)$_3$InCl$_6$.

the Pb-based HMHs. The intrinsic toxicity and weak moisture resistance severely limit their practical applications. Therefore, the exploitation of lead-free chiral HMHs with improved stability is of great significance.

In this case, In^{3+} has been demonstrated as a promising candidate for the substitution of the toxic Pb^{2+}. Due to the relatively small ionic radius, In^{3+}-based HMHs tend to form zero-dimensional (0D) structures, exhibiting excellent environmental stability [22,23]. For example, Lei *et al.* reported 0D [1,2-bis(3-aminopropylamino)ethane)]InCl$_6$·H$_2$O and (dipropylamine)$_3$InCl$_6$, which exhibited good structural and spectral stabilities after exposed in moisture atmosphere (>90% humidity) over one month [24]. Recently, SHG signal has also been observed in (*R*-methylphenethylamine)$_6$InCl$_9$ by Xu *et al.* [25]. Unfortunately, the indium halide is almost non-luminous. As we know, the multifunctional indium halides integrating SHG and CPL properties have never been documented.

Herein, we propose the molecular engineering strategies, namely chiral induction and Sb^{3+} doping, to achieve both SHG and CPL properties in lead-free indium halides. Specifically, two isostructural 0D In^{3+}-based HMHs ((*R*/*S*-MBA)$_3$InCl$_6$) were designed and synthesized by introducing chiral *R*/*S*-MBA as templating cations. The introduction of chiral cations can break the symmetry, and the (*R*/*S*-MBA)$_3$InCl$_6$ crystallize in chiral *P*1 space group, exhibiting obvious SHG responses. Moreover, by doping Sb^{3+}, broadband yellow emission can be turned on with photoluminescence quantum yield (PLQY) up to 86%. The spectroscopy and theoretical studies reveal the mechanism for the self-trapped excitons (STEs) emission. Combining the chirality and highly efficient luminescence, the as-prepared (*R*/*S*-MBA)$_3$InCl$_6$:Sb show not only SHG responses but also CPL signals with luminescence dissymmetry factor (g_{lum}) of -5.3×10^{-3} and 4.7×10^{-3}. This work not only enriches lead-free HMHs family, but also provides a new inspiration for the exploitation of chiral multifunctional materials.

Two isostructural chiral indium halides, (*R*-MBA)$_3$InCl$_6$ and (*S*-MBA)$_3$InCl$_6$, were synthesized by evaporating the ethanol precursor solution with stoichiometric *R*-MBA or *S*-MBA and InCl$_3$. (*R*-MBA)$_3$InCl$_6$ and (*S*-MBA)$_3$InCl$_6$ crystallized in the same chiral space group *P*1 with similar lattice parameters (the crystallographic data are summarized in Tables S1-S3 in Supporting information). (*R*-MBA)$_3$InCl$_6$ and (*S*-MBA)$_3$InCl$_6$ are isostructural, in which each In is coordinated with six Cl to form the distorted $[InCl_6]^{3-}$ octahedrons, and the $[InCl_6]^{3-}$ octahedrons are isolated and surrounded by *R*/*S*-MBA cations to form a 0D molecular geometry, as shown in Fig. 1. The shortest In-In distance exceeds 7 Å (7.306 Å for (*R*-MBA)$_3$InCl$_6$ and 7.310 Å for (*S*-MBA)$_3$InCl$_6$, indicating the negligible electronic interaction between adjacent $[InCl_6]^{3-}$ clusters [26]. Notably, the chiral organic cations are arranged orientally with the $-NH_3^+$ groups oriented towards the inorganic $[InCl_6]^{3-}$ octahedrons, which can be attributed to the N–H···Cl hydrogen bonds and

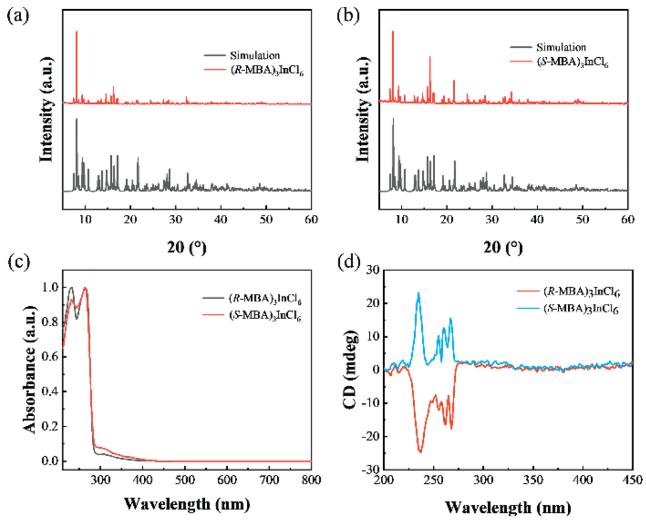

Fig. 2. The experimental and simulated PXRD patterns of (a) (*R*-MBA)$_3$InCl$_6$ and (b) (*S*-MBA)$_3$InCl$_6$. (c) The diffuse reflection absorption spectra of (*R*/*S*-MBA)$_3$InCl$_6$. (d) The CD spectra of (*R*/*S*-MBA)$_3$InCl$_6$.

coulomb interactions (Fig. S1). Owing to the asymmetric hydrogen bonds, the inorganic $[InCl_6]^{3-}$ octahedrons are asymmetrically tilted or distorted. These lattice distortions are clearly reflected on the Cl-In-Cl angles (Fig. S2 in Supporting information). Compared to the (*rac*-MBA)$_3$InCl$_6$, (*R*/*S*-MBA)$_3$InCl$_6$ show more obvious bond angle deviation. Furthermore, the bond angle variance (σ^2) and bond length distortion (Δd) were calculated to evaluate the degree of lattice distortion, and the results are listed in Table S4 (Supporting information). The σ^2 and Δd of (*R*/*S*-MBA) $_3$InCl$_6$ are higher than those of the previously reported achiral In-based HMHs, indicating the more distorted structures in the chiral indium halide [24,25,27-29]. As shown in Figs. 2a and b, the experimental powder XRD patterns of these two compounds are consistent with the simulated patterns, indicating that the as-prepared (*R*-MBA)$_3$InCl$_6$ and (*S*-MBA)$_3$InCl$_6$ are pure phases. In addition, thermogravimetric analysis (TGA) results suggest that these two homomorphic compounds exhibit good thermal stability, and the thermal decomposition temperature is higher than 200 °C (Fig. S3 in Supporting information).

To investigate the optical properties of (*R*/*S*-MBA)$_3$InCl$_6$, the UV-vis absorption spectra and CD spectra were measured. As shown in Fig. 2c, (*R*/*S*-MBA)$_3$InCl$_6$ show similar intense absorption peaks at about 231 and 263 nm, corresponding to the allowed E band and forbidden B band of π-π^* transition in MBA molecules, respectively [30,31]. In addition, the bandgaps can be calculated as about 4.44 eV by Tauc plot (Fig. S4 in Supporting information), in good agreement with their colorless and transparent nature under visible light, indicating the wide transparency windows and weak self-absorption under near-infrared laser pumping, which are attractive for SHG with high damage thresholds [32]. For CD measurement, the corresponding ethanol solution of (*R*/*S*-MBA)$_3$InCl$_6$ was spin-coated onto the quartz substrate. Fig. 2d depicts the CD spectra of (*R*/*S*-MBA)$_3$InCl$_6$, almost mirrored CD signals appear at 235 and 250–270 nm, which are agreement with the corresponding absorption peaks, confirming the chirality of (*R*/*S*-MBA)$_3$InCl$_6$.

The chiral space group promotes us to further investigate the SHG properties as SHG is dependent on the structural asymmetry [11]. For SHG measurements, the 1064 nm pulse laser was served as the pump. As shown in Fig. 3, obvious SHG signals can be observed at 532 nm, and the SHG intensity almost follows square relationship with the pumping power, revealing the second-order nonlinear optical properties [32]. In addition, the SHG intensity un-

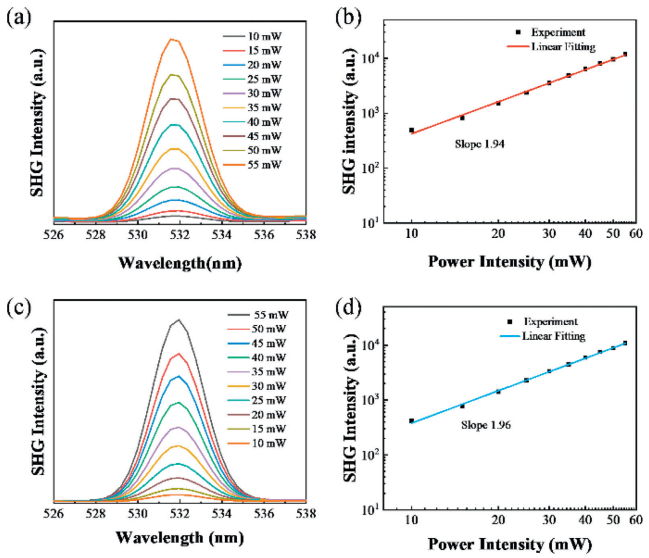

Fig. 3. SHG intensity of (a) (*R*-MBA)$_3$InCl$_6$ and (c) (*S*-MBA)$_3$InCl$_6$ under 1064 nm pump light. Logarithmic plot of SHG intensity as a function of the pumping power for (b) (*R*-MBA)$_3$InCl$_6$ and (d) (*S*-MBA)$_3$InCl$_6$.

der different polarization angle was measured to study the SHG anisotropy. As shown in Fig. S5 (Supporting information), the SHG intensity is polarization-dependent, and the SHG anisotropy ρ can be calculated to be about 0.97 according to Eq. 1 [33]:

$$\rho = (I_{max} - I_{min})/(I_{max} + I_{min}) \quad (1)$$

where I_{max} and I_{min} refer to the maximum and minimum SHG intensity. Such high ρ is coincident with structural asymmetry of (*R*/*S*-MBA)$_3$InCl$_6$. In addition, we also studied the circularly polarization properties of SHG. As shown in Fig. S6 (Supporting information), (*R*/*S*-MBA)$_3$InCl$_6$ exhibit different SHG intensity under left- or right-handed circularly polarized (LCP or RCP) light. The circularly polarization-resolved SHG effect can be quantified by the corresponding anisotropy factor (g_{SHG-CD}), which can be calculated by Eq. 2 [21]:

$$g_{SHG-CD} = |2(I_{LCP} - I_{RCP})|/(I_{LCP} + I_{RCP}) \quad (2)$$

where I_{LCP} and I_{RCP} refer to the SHG intensity under LCP and RCP light. The calculated g_{SHG-CD} values for (*R*/*S*-MBA)$_3$InCl$_6$ are about 0.43/0.44.

Materials showing CPL activity have attracted increasing attention owing to their potential applications in 3D displays, optical information processing, and sensing [34–37]. Chiral HMHs provide a versatile platform to integrate chiral units and luminescent units, and have been demonstrated as ideal candidates for CPL materials [13]. Unfortunately, (*R*/*S*-MBA)$_3$InCl$_6$ are almost non-luminous.

Doping has been considered as an effective means to regulate the emission properties of HMHs [8,38]. Antimony(III) halides featured the 5s^2 electron configuration usually exhibit highly efficient luminescence originating from the STEs [39–41]. In addition, Sb^{3+} possesses similar ionic radius and valence state with In^{3+}, and is expected to partially occupy the position of In^{3+} in the lattice without significantly changing the crystal structures [23,29]. Thus, Sb^{3+}-doping strategy was developed to improve the PLQY of the chiral indium halides. (*R*/*S*-MBA)$_3$InCl$_6$:Sb were synthesized in the same way as pure (*R*/*S*-MBA)$_3$InCl$_6$ with $InCl_3$ partially replaced by $SbCl_3$ (see the Experimental Section in Supporting information). As shown in Fig. S7 (Supporting information), the powder XRD patterns of (*R*/*S*-MBA)$_3$InCl$_6$:Sb match well with those of pure (*R*/*S*-MBA)$_3$InCl$_6$, indicating that the doping of Sb^{3+} does not obviously destroy the crystal structure [28]. The X-ray photoelectron spectroscopy results confirm the presence of relevant elements (Fig. S8 in Supporting information), and the doping ratio of Sb^{3+} was determined by inductively coupled plasma optical emission spectrometry (ICP-OES) to be 16.5% and 17.3%, respectively (Table S5 in Supporting information).

The photophysical properties of (*R*/*S*-MBA)$_3$InCl$_6$:Sb were characterized using UV-vis absorption spectra, as well as steady-state and transient-state photoluminescence (PL) spectra. As shown in Figs. 4a and d, Sb^{3+} doped (*R*/*S*-MBA)$_3$InCl$_6$ show similar absorption peaks to (*R*/*S*-MBA)$_3$InCl$_6$ at 230 and 265 nm, while additional absorption band appears at 280–400 nm, which can be assigned to the $^1S_0$-$^1P_1$ and $^1S_0$-$^3P_1$ transition of Sb^{3+} [23,24]. After Sb^{3+} doping, the bandgaps decrease to about 3.46 eV (Fig. S9 in Supporting information). Excitingly, (*R*/*S*-MBA)$_3$InCl$_6$:Sb exhibit bright orange-yellow emission under 365 nm excitation. The corresponding PL spectra show broadband emission centered at 610 nm with wide full width at half-maximum (FWHM) of 160 nm, and the Stokes shifts is up to 260 nm (Figs. 4b and e). The absolute PLQY of Sb^{3+} doped (*R*/*S*-MBA)$_3$InCl$_6$ was measured to be about 86% (Fig. S10 in Supporting information). The broadband emission with large Stokes shift is consistent with the characteristics of STEs emission, similar with the previously reported 0D HMHs [8]. The PL decay curves in Figs. 4c and f exhibit long decay time of 3.98 and 4.04 μs for (*R*/*S*-MBA)$_3$InCl$_6$:Sb, respectively, indicating that the emission comes from the excited triplet state.

The temperature-dependent emission spectra were further investigated to support the STEs emission mechanism, as the electron-phonon coupling is sensitive to temperature [42,43]. As the temperature increases, the emission intensity decreases and the FWHM widens (Fig. S11 in Supporting information), indicating that the coupling of electron-phonon is enhanced, which promotes non-radiative recombination [44]. In addition, there is slight red-shift in emission peak with increasing temperature, which can be ascribed to the synergistic effects of electron-phonon coupling and thermal lattice expansion [45].

To reveal the effect of Sb^{3+} doping on photophysical properties, the electronic structures of undoped and Sb^{3+} doped (*R*/*S*-MBA)$_3$InCl$_6$ were calculated (Figs. S12 and S13 in Supporting information). The theoretical calculated bandgap values of (*R*/*S*-MBA)$_3$InCl$_6$:Sb are about 2.98 eV, smaller than those of undoped (*R*/*S*-MBA)$_3$InCl$_6$ (about 3.42 eV), which are consistent with the trend of experimental results. The calculated density of states (DOS) shows that the conduction band minimum (CBM) of (*R*/*S*-MBA)$_3$InCl$_6$ and (*R*/*S*-MBA)$_3$InCl$_6$:Sb are both contributed by the In-s and Cl-p states. Differently, the valence band maximum (VBM) of (*R*/*S*-MBA)$_3$InCl$_6$ is dominated by the organic cations, while (*R*/*S*-MBA)$_3$InCl$_6$:Sb have some relatively higher energy levels in the valence bands, dominated by the Sb-s and Cl-p orbitals. The charge density distributions of (*R*/*S*-MBA)$_3$InCl$_6$ and (*R*/*S*-MBA)$_3$InCl$_6$:Sb have also been calculated (Figs. S14 and S15 in Supporting information). For (*R*/*S*-MBA)$_3$InCl$_6$, the charge carriers in the CBM are localized in the $[InCl_6]^{3-}$ polyhedrons, whereas the charge carriers in the VBM are localized in the organic cations. After Sb^{3+} doping, the charge carriers of both VBM and CBM are localized in the inorganic polyhedrons, and there is no obvious electronic band between the adjacent inorganic polyhedrons, indicating the strong quantum confinement effect. Furthermore, the effective electron- and hole-mass have increased after doping Sb^{3+} (Table S6 in Supporting information), which is favorable for the formation of the STEs [40,46]. These results demonstrate that Sb^{3+} dopants have obvious effect on the electronic structures, resulting in the enhanced emission.

Similar with the (*R*/*S*-MBA)$_3$InCl$_6$, CD and SHG signals can also be detected in Sb^{3+} doped (*R*/*S*-MBA)$_3$InCl$_6$, further demonstrating the chiral structures (Fig. 5a and Fig. S16 in Supporting information). Combining the chiral structures and the excellent emis-

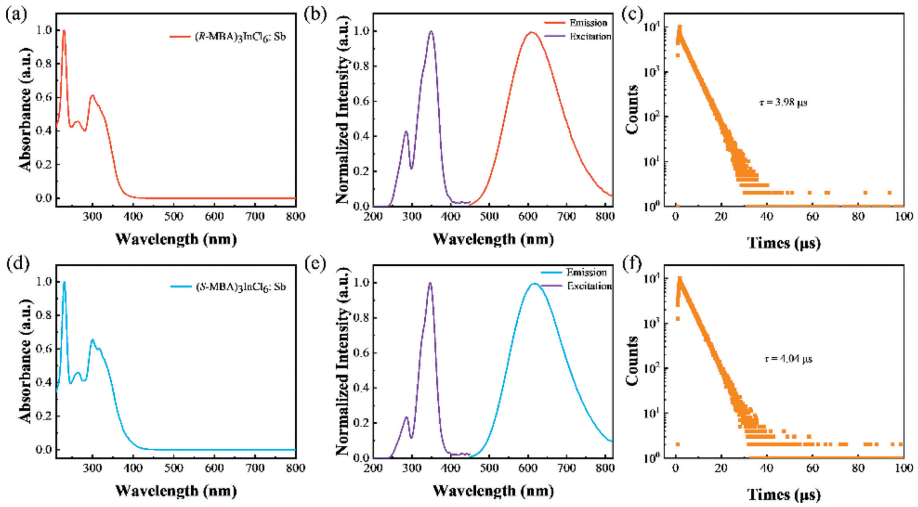

Fig. 4. UV-vis diffuse reflectance absorption spectra of (a) (*R*-MBA)$_3$InCl$_6$:Sb and (d) (*S*-MBA)$_3$InCl$_6$:Sb. Excitation and emission spectra of (b) (*R*-MBA)$_3$InCl$_6$:Sb and (e) (*S*-MBA)$_3$InCl$_6$:Sb. PL decay lifetimes of (c) (*R*-MBA)$_3$InCl$_6$:Sb and (f) (*S*-MBA)$_3$InCl$_6$:Sb.

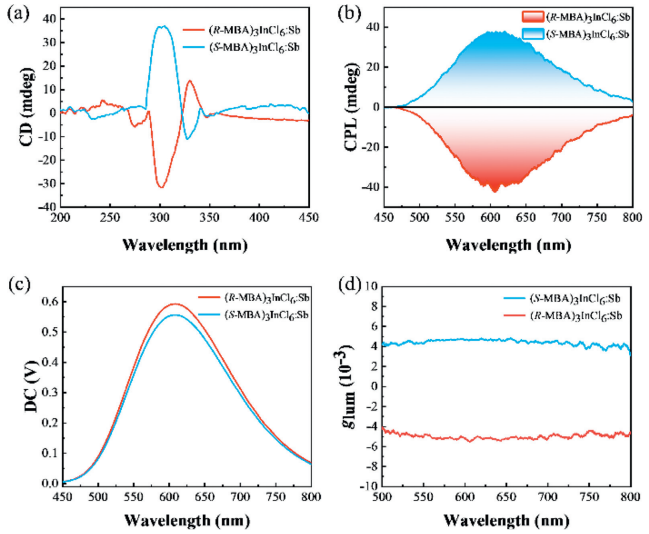

Fig. 5. (a) CD spectra of (*R*/*S*-MBA)$_3$InCl$_6$:Sb. (b) The CPL spectra of (*R*/*S*-MBA)$_3$InCl$_6$:Sb. (c) The DC spectra of (*R*/*S*-MBA)$_3$InCl$_6$:Sb. (d) The g_{lum} of (*R*/*S*-MBA)$_3$InCl$_6$:Sb.

sion properties, we further explored the CPL behaviors of (*R*/*S*-MBA)$_3$InCl$_6$:Sb. As shown in Figs. 5b and c, the CPL spectra are coincided well with the PL spectra, suggesting that the chiral-optical properties in the excited state are also originated from the STEs emission [38]. Sb^{3+} doped (*R*-MBA)$_3$InCl$_6$ and (*S*-MBA)$_3$InCl$_6$ exhibit opposite CPL signals, consistent well with the corresponding chirality. The g_{lum}, which quantifies the asymmetry degree of emission in LCP and RCP light, is an important parameter to evaluate the CPL performance, and can be calculated by Eq. 3 [38,47]:

$$g_{lum} = 2(I_L - I_R)/(I_L + I_R) \quad (3)$$

where I_L and I_R mean the intensity of left- and right-CPL, respectively. For the application of CPL, high PLQY and $|g_{lum}|$ are desired, and the higher PLQY and $|g_{lum}|$ mean the lower energy loss. The g_{lum} values of (*R*-MBA)$_3$InCl$_6$:Sb and (*S*-MBA)$_3$InCl$_6$:Sb are measured to be -5.3×10^{-3} and 4.7×10^{-3} (Fig. 5d), respectively, which are on par with those of chiral lead(II) halides [48–51].

In summary, we have successfully designed and synthesized two isostructural 0D chiral In^{3+}-based HMHs ((*R*/*S*-MBA)$_3$InCl$_6$) using chiral amine as templating cation. Induced by the chiral cations, (*R*/*S*-MBA)$_3$InCl$_6$ crystallize in chiral *P*1 space groups, thus exhibiting remarkable SHG responses under 1064 nm pump light. After doping with Sb^{3+}, the PL emission is turned on with PLQY up to 86%. The experimental and theoretical studies reveal that the Sb^{3+} dopants have significant contribution to the frontier orbitals and the PL emission is derived from the radiative recombination of STEs. Notably, the doping of antimony does not destroy the crystal structures, and the chiral structures can be retained in the (*R*/*S*-MBA)$_3$InCl$_6$:Sb, so that SHG signals can still be detected. Excitingly, CPL signals can be detected with g_{lum} of -5.3×10^{-3} and 4.7×10^{-3}. We believe this work could provide some inspirations for exploring and designing novel lead-free metal halides toward chiral optical applications.

Declaration of competing interest

The authors declare that they have no known competing financial interests or personal relationships that could have appeared to influence the work reported in this paper.

Acknowledgments

This work was supported by the National Funds for Distinguished Young Scientists (No. 61825503) and the National Natural Science Foundation of China (Nos. 62288102, 62375142 and 22161160318).

Supplementary materials

Supplementary material associated with this article can be found, in the online version, at doi:10.1016/j.cclet.2023.109085.

References

[1] D. Yan, Z.F. Wang, Z.J. Zhang, Acc. Chem. Res. 55 (2022) 1047–1058.
[2] W.M. Awad, D.W. Davies, D. Kitagawa, et al., Chem. Soc. Rev. 52 (2023) 3098–3169.
[3] P. Tao, S.J. Liu, W.Y. Wong, Adv. Opt. Mater. 8 (2020) 2000985.
[4] F.Y. Li, X. Wen, Z.Z. Xue, et al., Cryst. Growth Des. 22 (2022) 4601–4609.
[5] H. Peng, Q. Liu, Y.H. Liu, et al., Chin. Chem. Lett. 34 (2022) 107980.
[6] Z. Wang, X.Y. Zhang, J.T. Mo, et al., Adv. Opt. Mater. 11 (2023) 2203144.
[7] Z. Wang, J.T. Mo, J.J. Pan, et al., Adv. Funct. Mater. 33 (2023) 2300021.
[8] C.K. Zhou, L.J. Xu, S.J. Lee, et al., Adv. Opt. Mater. 9 (2020) 2001766.
[9] L.J. Du, T. Hasan, A. Castellanos-Gomez, et al., Nat. Rev. Phys. 3 (2021) 193–206.
[10] P.P. Shi, Y.Y. Tang, P.F. Li, et al., Chem. Soc. Rev. 45 (2016) 3811–3827.

[11] J.L. Xu, X.Y. Li, J.B. Xiong, et al., Adv. Mater. 32 (2020) 1806736.
[12] T.H. Zhao, J.L. Han, Y.H. Shi, et al., Adv. Mater. 33 (2021) 2101797.
[13] Y.Y. Dang, X.L. Liu, B.Q. Cao, et al., Matter 4 (2021) 794–820.
[14] D.G. Billing, A. Lemmerer, Acta Crystallogr. Sect. E: Struct. Rep. Online 59 (2003) m381.
[15] J. Ahn, E. Lee, J.W. Tan, et al., Mater. Horiz. 4 (2017) 851–856.
[16] J.R. Zhang, X.F. Song, L. Wang, et al., Natl. Sci. Rev. 9 (2022) nwab129.
[17] C.X. Li, P.F. Duan, Chem. Lett. 50 (2021) 546–552.
[18] J.Q. Ma, C. Fang, C. Chen, et al., ACS Nano 13 (2019) 3659–3665.
[19] W.J. Chen, S. Zhang, M.H. Zhou, et al., J. Phys. Chem. Lett. 10 (2019) 3290–3295.
[20] Y. Peng, Y.P. Yao, L.N. Li, et al., J. Mater. Chem. C 6 (2018) 6033–6037.
[21] D.Y. Fu, J.L. Xin, Y.Y. He, et al., Angew. Chem. Int. Ed. 60 (2021) 20021–20026.
[22] D. Chen, S.Q. Hao, G.J. Zhou, et al., Inorg. Chem. 58 (2019) 15602–15609.
[23] D.H. Liang, X.H. Liu, B.B. Luo, et al., Ecomat 5 (2023) e12296.
[24] C. Sun, J.P. Zang, Y.Q. Liu, et al., CCS Chem. 4 (2022) 3106–3121.
[25] S.M. Qi, F. Ge, X. Han, et al., Dalton Trans. 51 (2022) 8593–8599.
[26] S.G. Zhou, L. Zhou, Y.H. Chen, et al., J. Phys. Chem. Lett. 13 (2022) 8717–8724.
[27] X.S. Zhang, X.X. Jiang, K.J. Liu, et al., Inorg. Chem. 61 (2022) 7560–7567.
[28] F. Lin, G.C. Yu, S.C. Weng, et al., Mater. Chem. Front. 7 (2022) 137–144.
[29] Y. Wu, C.M. Shi, S.R. Kang, et al., Inorg. Chem. Front. 9 (2022) 5008–5015.
[30] Y. Lu, Q. Wang, R.L. He, et al., Angew. Chem. Int. Ed. 60 (2021) 23578–23583.
[31] L. Yao, G.D. Niu, J.Z. Li, et al., J. Phys. Chem. Lett. 11 (2020) 1255–1260.
[32] F. Ge, B.H. Li, P.X. Cheng, et al., Angew. Chem. Int. Ed. 61 (2022) e202115024.
[33] L.L. Zhao, X. Han, Y.S. Zheng, et al., Adv. Photonics Res. 2 (2021) 2100056.
[34] Y.J. Deng, M.Z. Wang, Y.L. Zhuang, et al., Light: Sci. Appl. 10 (2021) 76.
[35] Y.T. Sang, J.L. Han, T.H. Zhao, et al., Adv. Mater. 32 (2019) 1900110.
[36] P. Fan, Z. Fang, S.Y. Wang, et al., Chin. Chem. Lett. 34 (2023) 107934.
[37] Z.L. Gong, X.F. Zhu, Z.H. Zhou, et al., Sci. China Chem. 64 (2021) 2060–2104.
[38] Z.Y. Wang, X.M. Wang, Z.W. Chen, et al., Angew. Chem. Int. Ed. 62 (2023) e202215206.
[39] Y.Y. Jing, Y. Liu, M.Z. Li, et al., Adv. Opt. Mater. 9 (2021) 2002213.
[40] Y.J. Deng, X. Liang, F.Y. Li, et al., Laser Photonics Rev 17 (2023) 2300043.
[41] H.X. Meng, B. Chen, W.J. Zhu, et al., Laser Photonics Rev. 17 (2023) 2201007.
[42] D.Y. Li, Y. Cheng, Y.H. Hou, et al., J. Mater. Chem. C 10 (2022) 3746–3755.
[43] J.L. Li, Y.F. Sang, L.J. Xu, et al., Angew. Chem. Int. Ed. 60 (2021) e202113450.
[44] H.L. Xuan, J.L. Li, L.J. Xu, et al., Adv. Opt. Mater. 10 (2022) 2200591.
[45] L.K. Gong, J.R. Li, Z.F. Wu, et al., J. Mater. Chem. C 7 (2019) 9803–9807.
[46] G.M. Song, M.Z. Li, S.Z. Zhang, et al., Adv. Funct. Mater. 30 (2020) 2002468.
[47] M.Z. Wang, X.M. Wang, B.T. Zhang, et al., J. Mater. Chem. C 11 (2023) 3206–3212.
[48] X.H. Zhao, X.Z. Hu, M.E. Sun, et al., J. Mater. Chem. C 10 (2022) 3440–3446.
[49] K.H. Jin, Y. Zhang, K.J. Li, et al., Angew. Chem. Int. Ed. 61 (2022) e202205317.
[50] Y. Peng, X. Wang, L.N. Li, et al., Adv. Opt. Mater. 11 (2022) 2201888.
[51] J.T. Lin, D.G. Chen, L.S. Yang, et al., Angew. Chem. Int. Ed. 60 (2021) 21434–21440.